Applied Physics Letters

Giant enhancement of plasmonic response and epsilon-near-zero signature in refractory transition metals (Ta, W, and Mo) deposited at high-temperature

Cite as: Appl. Phys. Lett. **118**, 041902 (2021); https://doi.org/10.1063/5.0027497
Submitted: 29 August 2020 . Accepted: 14 January 2021 . Published Online: 28 January 2021

Krishna Chand Maurya, Bidesh Biswas, Dheemahi Rao, and Bivas Saha

Applied Physics Letters ARTICLE scitation.org/journal/apl

Giant enhancement of plasmonic response and epsilon-near-zero signature in refractory transition metals (Ta, W, and Mo) deposited at high-temperature

Cite as: Appl. Phys. Lett. **118**, 041902 (2021); doi: 10.1063/5.0027497
Submitted: 29 August 2020 · Accepted: 14 January 2021 ·
Published Online: 28 January 2021

Krishna Chand Maurya,[1,2,3] Bidesh Biswas,[1,2,3] Dheemahi Rao,[1,2,3] and Bivas Saha[1,2,3,a)]

AFFILIATIONS

[1]Chemistry and Physics of Materials Unit, Jawaharlal Nehru Centre for Advanced Scientific Research, Bangalore 560064, India
[2]International Centre for Materials Science, Jawaharlal Nehru Centre for Advanced Scientific Research, Bangalore 560064, India
[3]School of Advanced Materials, Jawaharlal Nehru Centre for Advanced Scientific Research, Bangalore 560064, India

[a)]**Author to whom correspondence should be addressed:** bsaha@jncasr.ac.in and bivas.mat@gmail.com

ABSTRACT

In recent years, the plasmonic materials with high optical loss ushered many innovations, such as loss-induced heating, plasmon-induced hot carrier, and electro-thermo-plasmonic nanotweezers. Similarly, epsilon-near-zero (ENZ) materials that exhibit near-zero real-components of the dielectric permittivity (ε_1) with high loss are promising for efficient absorbers, hot-electron generation, photo-catalysis, local heating, nanoparticle trapping, etc. Traditionally, the plasmonic and ENZ materials based on noble metals such as Au and Ag are not stable at high-temperatures, are CMOS incompatible, and exhibit ENZ behavior in a narrow wavelength range, whereas though transition metal nitrides such as TiN and ZrN exhibit ENZ in the visible spectrum, their spectral width is rather small. Therefore, ENZ materials that are broadband in nature, refractory, oxidation resistant, and CMOS compatible should exhibit better device performance and are highly desired. In this letter, we demonstrate epitaxial, highly crystalline refractory transition metals (RTMs) such as Ta, W, and Mo deposited at high-temperatures (700 °C) in ultra-high vacuum ($\sim 2 \times 10^{-9}$ Torr), which exhibit broadband ENZ characteristics with relatively flat ε_1 in the visible-to-near-IR spectral ranges (200 nm–1000 nm). Phase-pure high crystalline-quality and smooth surfaces result in more metallicity, which leads to a large negative ε_1 in long-wavelength (1000 nm–2500 nm) ranges that are comparable to the ε_1 of alternative plasmonic materials such as TiN and ZrN. Plasmonic and ENZ characteristics are found to be robust at high-temperatures (~700 °C) and result in enhanced optical absorption in the RTM metasurface that would be useful for thermophotonic energy conversion, nonlinear optics, and nonreciprocal optical devices.

Traditionally, plasmonic materials that exhibit negative real components of the dielectric permittivity (ε_1) and very small imaginary components of the dielectric permittivity (ε_2) or optical losses were regarded as ideal candidates for the demonstration of the interesting and exotic optical phenomenon and for the practical device implementations.[1] However, in recent years, it is realized that higher ε_2 in plasmonic materials is essential[2,3] for the confinement and impedance effects[4] such as loss-induced heating,[5] plasmon-induced hot carrier,[6] and electro-thermo-plasmonic nanotweezer.[7] At the same time, epsilon-near-zero (ENZ) materials that exhibit ε_1 close to zero[8] in certain wavelength ranges are developed, which has brought many possibilities in nanophotonic devices.[9–11] ENZ materials with large optical losses can be useful as efficient absorbers,[12] hot-electron generation,[13] nanoparticle trapping,[14,15] photo-catalysis,[16] solar-thermophotovoltaics,[17,18] etc. If the ENZ materials are also accompanied by small optical losses, such materials also exhibit near-zero-index[4] (NZI) and a host of interesting and exotic optical properties such as photon tunneling,[19,20] super-coupling,[21] extreme nonlinear interactions,[22] ultrafast switching,[23] and optical nanocircuits.[24] As the ENZ region corresponds to the bulk plasma frequency [with a corresponding crossover wavelength ($\lambda_{co.}$) at which the sign of ε_1 changes from positive to negative and/or the wavelength at which $\varepsilon_1 = 0$], the carrier concentration of the materials plays an extremely important role in determining the ENZ spectral range. Several classes of materials such as metals (for example, Ag and Au),[25] semimetals (ZrSiS,[26] TaAs,[27] and Na_3Bi[27]), doped semiconductors (ITO[28] and Al:ZnO[23]), polaritonic materials

(such as SiC[29]), and metamaterials[30] show ENZ behavior in different electromagnetic spectral ranges.

Conventional noble metals such as Au[25] ($\lambda_{co.} = 510$ nm) and Ag[25] ($\lambda_{co.} = 310$ nm), which exhibit ENZ characteristics in the visible and near-UV spectral range due to their large carrier concentrations ($\geq 10^{20}$ cm^{-3}), exhibit sharp ENZ regions and are not suitable for practical refractory applications due to their softness,[31] the low melting temperature of nanostructures,[31] CMOS incompatibility,[32] and inability to deposit them in the thin and ultrathin smooth film (<10 nm).[33,34] Though recently developed transition metal nitrides such as TiN[35,36] ($\lambda_{co.} = 450$ nm–500 nm) and ZrN[35] ($\lambda_{co.} \approx 410$ nm), on the other hand, overcome some of the limitations of noble metals, their spectral ENZ regions are rather narrow. Metal/dielectric multilayers such as Ag/TiO_2[37] and TiN/$Al_{0.72}Sc_{0.28}N$[38] superlattices also exhibit ENZ properties in the visible spectral range with some degree of tunability, though they require advanced nanofabrication methods to develop. Therefore, there is a wide-scale requirement for broadband ENZ materials that are refractory in nature and are also structurally, mechanically, and morphologically stable at high temperature, CMOS compatible, and rather easy to deposit and develop for industrial applications.

Refractory transition metals (RTMs) such as Ta, W, and Mo are corrosion resistant, mechanically hard, and actively used for a range of industrial applications such as in incandescent light bulb filaments, x-ray tubes, gas turbines, capacitors in the electronic industry, and radiation shielding.[39] In addition, RTMs also exhibit some of the largest melting temperature in materials, Ta (3017 °C), W (3422 °C), and Mo (2633 °C), and are stable against creep deformation at high temperatures.[39] Due to the metallic nature, RTMs exhibit very low electrical resistivity Ta (135 n Ω m), W (50 n Ω m), and Mo (53 n Ω m) at room temperature.[39] Low diffusivities in silicon (Si) also make RTMs useful for Si-technology; for example, Ta has been used as a diffusion barrier in VLSI (Very Large Scale Integration) technology for preventing Cu from penetrating into Si.[40] Smooth patterned nanostructures of RTMs have been shown for various photonic applications such as absorbers,[41] thermal emitters,[42] photonic crystals,[43] and thermophotovoltaics,[18] albeit with not so good material and optical properties. Therefore, RTMs have the potential to be a new class of materials for the plasmonic, ENZ, and photonic devices especially for refractory applications, and it is natural to investigate the optical properties of RTMs and engineer their plasmonic characteristics and ENZ behavior. Unfortunately, there are only a handful of reports on the optical properties of RTMs,[44,45] which do not show promising plasmonic and ENZ characteristics. Though there are some scattered reports on the epitaxial growth of RTMs (Ta,[46] W,[47] and Mo[48]) at high substrate temperature, almost all the optical characterization of RTMs relies on room-temperature deposited films that are polycrystalline in nature and exhibit little-to-no plasmonic response (see supplementary material 11). Therefore, with the motivation to develop RTMs as the plasmonic and ENZ materials, in this article, we demonstrate high-temperature deposited Ta, W, and Mo thin films that exhibit broadband ENZ behavior accompanied by high-quality plasmonic characteristics in the visible-to-near-IR spectral range. The high substrate temperature during depositions increases adatom mobility necessary to overcome the Ehrlich–Schwoebel, surface diffusion, and grain boundary activation barriers and results in impurity free smooth films with high crystalline quality[49,50] that increases the intrinsic carrier concentration and carrier mobility while decreasing the carrier scattering that results in optical losses.

RTM (Ta, W, and Mo) thin films were deposited on (001) MgO and (0001) Al_2O_3 substrates with reactive rf-magnetron sputtering (PVD Products Inc.) (see the supplementary material for details). Two sets of samples with a substrate held at (a) room temperature (30 °C) denoted as RT and (b) 700 °C denoted as HT (high temperature) were deposited. All films under investigation are ∼100 nm thick. As films deposited on MgO and Al_2O_3 substrates show similar results, most of the results presented in the manuscript are from films deposited on MgO substrates. The ambient temperature optical characterization was performed with a variable angle spectroscopic ellipsometer, and the experimental (ψ, Δ) spectra were fitted with a combination of the Drude–Lorentz model (see supplementary material 2 for details).

The results show that all RTM films (see Fig. 1) exhibit plasmonic behavior ($\varepsilon_1 < 0$) in the near IR spectral ranges that are accompanied by ENZ regions. The spectral position and the nature of ENZ, however, depend not only on the metals under investigation but also on the growth conditions. RT-deposited films are found to exhibit double ENZ characteristics, i.e., the sign of ε_1 changing from negative-to-positive and vice versa in the UV and near-IR spectral ranges, respectively. For example, in RT-Ta, the double ENZ regions are found to be at 210 nm and 1410 nm, while for RT-Mo and for RT-W, the ENZ points are located at 210 nm and 1200 nm and at 254 nm and 880 nm, respectively. Optical losses (ε_2) corresponding to such ENZ points are found to be 4.14 and 9.94 for RT-Ta, 3.17 and 9.48 for RT-Mo, and 4.79 and 12.7 for RT-W. After the ENZ region in the near-IR (when ε_1 changed from positive-to-negative), all three RTMs exhibit negative ε_1 characteristic of their plasmonic nature. RT-W is found to exhibit the largest negative ε_1 among the three metals primarily due to its larger carrier concentrations that were verified with its larger Drude plasma frequency (ω_p) (see Table S1 in the supplementary material). Optical losses of RT-W, however, are larger compared to those of the other two films.

Compared to the RT-RTMs, high-temperature deposited metals exhibit significantly larger negative ε_1 in the near-IR spectral range and relatively higher optical losses (ε_2). For example, at 2500 nm, ε_1 in RT-Ta was measured to be −7, while that of HT-Ta is −140 [see Fig. 1(a)]. In addition, with their larger ε_1, optical loss or ε_2 of the HT-RTM films is also much higher [see Fig. 1(b)]. Larger ε_1 and ε_2 in HT films can be explained by the Drude model in Eq. (1) that represents the free-electron response, where

$$\varepsilon = \varepsilon_1 + i\varepsilon_2 = 1 - \frac{\omega_p^2}{\omega^2 + i\,\Gamma_D \omega}, \tag{1}$$

$$\varepsilon_1 = 1 - \frac{\omega_p^2}{\omega^2 + \Gamma_D^2}, \tag{2}$$

$$\varepsilon_2 = \frac{\omega_p^2 \Gamma_D}{\omega^3 + \Gamma_D^2 \omega}. \tag{3}$$

Fitting of the experimental results shows (see Table S1 of the supplementary material) that ω_p is significantly larger in HT-RTMs than that in RT-RTMs due to their larger number of free carriers and leads to larger ε_1 and ε_2. For example, compared to a ω_p of 3.41 eV in RT-Ta, HT-Ta exhibits about two times larger ω_p of 6.85 eV. Similarly, the relatively flat ε_1 in HT-RTMs results from the total

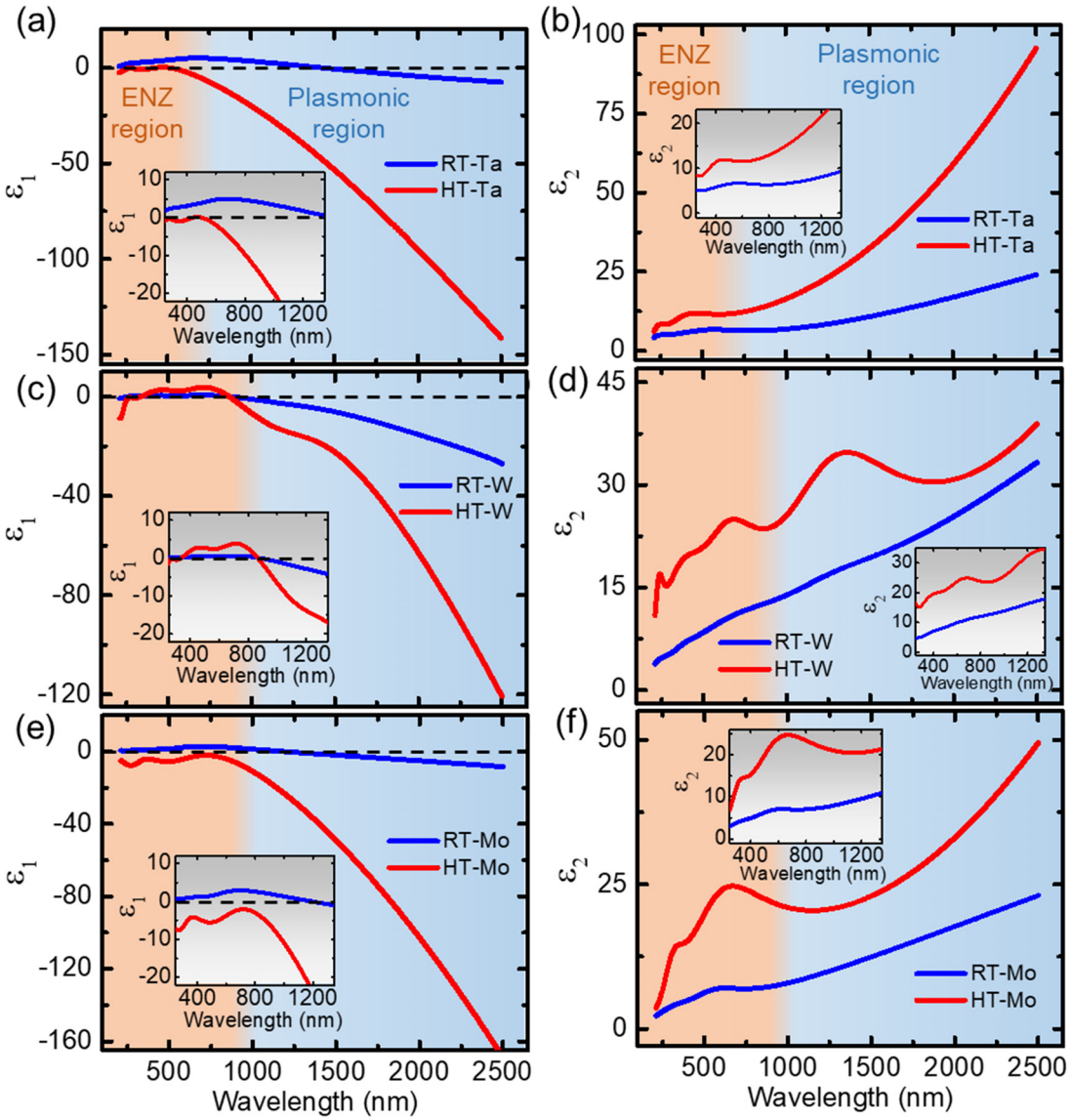

FIG. 1. The optical property of refractory transition metals (RTMs) is presented. (a), (c), and (e) The real (ε_1) and (b), (d), and (f) imaginary (ε_2) parts of the dielectric permittivity of sputter-deposited transition metal (Ta, W, and Mo) thin films on MgO substrates at 25 °C (RT) and 700 °C (HT) substrate temperatures. The inset shows ENZ regions and double-ENZ behavior of the films. The optical response (ε_1) of HT-RTM films is significantly larger than that of RT-RTMs, and consequently, optical loss (ε_2) is also large. Note: the color gradient in the figures is according to the HT-RTMs.

contribution of inter-band transitions, intra-band transitions, or additional scattering losses due to defects in RTMs in the 210 nm–1200 nm spectral range, which leads to large Lorentz damping constant (see Table S1 of the supplementary material) and does not allow a monotonic decrease in ε_1 with the increase in the wavelength. Flatter ε_1 and its value close to zero make HT-RTMs better suited for several ENZ applications with a broader spectral operation range. For example, in HT-Ta ENZ, the wavelength ranged (corresponding to $-2 < \varepsilon_1 < 2$) from 230 nm to 600 nm, while in HT-W ENZ, wavelengths encompassed the 340 nm to 865 nm spectral region. Though the ENZ regions of the HT-RTMs are broad, the corresponding optical losses are found to be large at 7.6 to 11 for HT-Ta [see Fig. 1(a)] and 5.9 to 12.4 for HT-W [see Fig. 1(c)], respectively. While such large optical losses prevent the HT-RTMs to achieve NZI, they should be conducive for a range of confinement and impedance effects in ENZ regions.

To understand the origin of superior metallic (plasmonic) and ENZ behavior in HT-RTMs, reflectivity measurements and detailed materials characterization with high-resolution x-ray diffraction (HRXRD) and atomic force microscopy (AFM) are performed (see Fig. 2 for Ta that is representative for other metals). The symmetric 2 θ-ω HRXRD diffractogram of HT-Ta showed a peak at 38.26° representing its (110) oriented growth on (002) MgO substrates

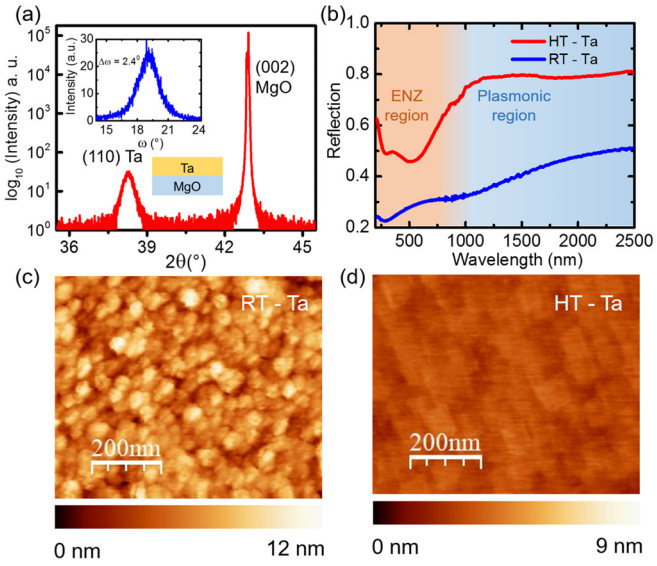

FIG. 2. (a) Symmetric 2 $\theta - \omega$ x-ray diffractogram of HT-Ta/MgO thin films along with their rocking curve (ω-scan) in the inset. Ta was found to grow with (110) orientations on the (002) MgO substrate. The FWHM ($\Delta\omega$) of the rocking curve was found to be 2.4° in the HT-Ta/MgO film, and (b) the HT-Ta film exhibits much higher reflectivity and a sharp dip close to ENZ regions compared to RT-Ta. Atomic force micrographs (AFM) show the RMS-surface roughness of (c) 1.6 nm in the RT-Ta film and (d) 0.5 nm in the HT-Ta film, respectively.

[see Fig. 2(a)]. The full-width-at-the-half-maxima (FWHM) of the rocking curve is found to be 2.4° in the HT-Ta/MgO film, which represents its nominal single crystalline nature. From the HRXRD analysis, it appears that HT-Ta crystalizes in the body-centered cubic α-Ta phase with a space group $Im\bar{3}m$ (229) and a lattice constant of 3.32 Å. XRD analysis on RT-Ta exhibits a peak at 37.2° that corresponds to the (111) oriented growth of the β-Ta phase and represents a lattice constant of 3.41 Å (see supplementary material 6). Bulk Ta crystalizes in the α-Ta phase, while β-Ta is usually obtained in physical vapor deposited films at low temperatures. Increasing the temperature of β-Ta to more than 700 °C converts it to the α-phase that was observed[51] previously. Therefore, the high-temperature growth at 700 °C in this work directly results in the α-Ta phase. The XRD peak intensity is significantly larger, and the peak width is much smaller for HT-Ta than for RT-Ta that represents its excellent crystal quality. Therefore, the superior optical properties of HT-Ta are not only due to its better crystalline quality but also due to its different crystal structure. HT-Ta exhibits ∼80% reflectivity in the near-IR spectral range and a sharp dip in reflection below 1000 nm, representing its plasmonic characteristics. In comparison, RT-Ta exhibits much smaller reflection (40%) and a less pronounced dip that correlates well with its significantly smaller ε_1 [see Fig. 2(b)] compared to HT-Ta. Atomic force micrographs showed that HT-RTM surfaces are much smoother, with the RMS-surface roughness of 0.5 nm, while that of RT-Ta was found to be 1.6 nm [see Figs. 2(c) and 2(d)].

Having addressed the origin of plasmonic properties and ENZ behavior in HT-Ta, temperature-dependent optical properties are measured with a cryostat attached with the ellipsometer in the 100 K to 700 K temperature range at an angle of incidence of 70 °. The cryostat chamber was attached with a turbo-molecular pump, leading to a chamber pressure of 10^{-7} Torr that would reduce possibilities of oxidation of the films.

The results show that with an increase in temperature, the magnitude of ε_1 of the HT-Ta film decreased monotonically, while the optical loss or ε_2 increased significantly in the near-IR spectral range [see Figs. 3(a) and 3(b)]. For example, with an increase in temperature from 100 K to 700 K, the magnitude of ε_1 at 2500 nm decreased from −110 to −68, while ε_2 increased from 90 to 117 for the same amount of change in temperature at 2500 nm. In the visible spectral range, ε_1 did not change appreciably, suggesting that the inter-band transition pathways and cross sections remain relatively unchanged within the measured temperature range. Since most of the changes in the permittivity occur in the near-IR spectral range, the Drude model is used to explain the observed behavior. The plasma frequency (ω_p) in the Drude model is related to the carrier concentration (N) and effective mass (m^*) through the relationship $\omega_p^2 = \frac{Ne^2}{m^*\epsilon_0}$. With an increase in temperature, the carrier density (N) usually decreases due to the volume expansion and the electron effective mass decreases.[52] A larger decrease in the effective mass of the electron, compared to the decrease in electron density due to expansion in the lattice, is responsible for the increment of plasma frequency with temperature. Also, the thermal population of carriers might be responsible for the increment of the plasma frequency. The Drude damping constant (Γ_D) increases with temperature due to the increment in the rate of various scattering mechanisms with temperature such as electron–electron scattering and electron–phonon scattering.[53]

ω_p and Γ_D have been extracted from the temperature-dependent optical constant and are presented in Fig. 3(c), which shows that both of them increase with an increase in temperature. The decrease in the magnitude of ε_1 in long-wavelength regions with the increase in temperature is related to the increase in both ω_p and Γ_D through Eq. (3). On the other hand, the increase in Γ_D and ω_p with temperature is responsible for the increase in ε_2 through Eq. (4). The temperature-dependent optical properties of HT-W and HT-Mo also show similar behavior as HT-Ta (see supplementary material 4). Several other plasmonic materials such as Au,[54] Ag,[55] and TiN[56] thin films have exhibited similar temperature-dependent plasmonic properties.

For the practical implementation of the RTMs, metasurface absorbers based on the RTM-dielectric-RTM heterostructure are simulated [see a unit cell of the metasurface in Fig. 4(a)] by utilizing the experimental data. The thickness of the bottom RTM and top RTM and width of the top RTM were fixed at 150 nm, 100 nm, and 500 nm, respectively. The thickness of the dielectric layer (Al_2O_3) was fixed at 50 nm. The metal–insulator–metal (MIM) structure acts as an optical cavity (see supplementary material 7 for details). The absorption spectrum of a 100 nm bare W film was also calculated (green curve), which agrees well with the experimental measurement (pink-dots) [see Fig. 4(d)], thus benchmarking the calculation methodology. Absorption calculated for the metasurface structure exhibits significant enhancement (almost reaching to ideal values for certain wavelengths) over the bare RTM film [see Fig. 4(c)], and the absorption peaks are also tuned with changing the dielectric layer thickness [see Fig. 4(d)]. A redshift in the absorption peak was observed with an increase in the dielectric layer thickness due to Fabry–Pérot resonance.[57] While the metasurface based on these three HT-RTMs exhibits similar absorption in the visible spectral range, the HT-W based metasurface

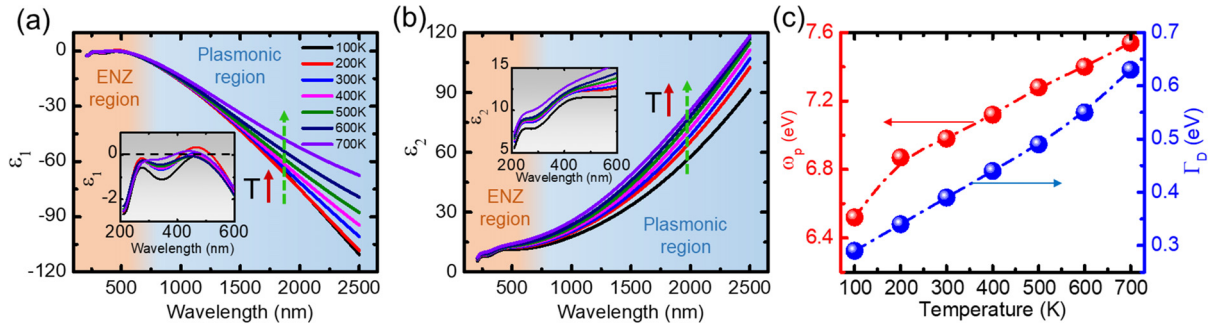

FIG. 3. Temperature-dependent real (ε_1) (a) and imaginary (ε_2) (b) components of the dielectric permittivity of the HT-Ta film, which shows that with an increase in temperature (100 K–700 K), ε_1 decreases, while ε_2 increases due to an increase in Drude damping constants and plasma frequency in long wavelength ranges. In the visible and near IR range, ε_1 remains almost unchanged with a small increase in optical loss. The inset shows the ENZ region that does not change much with temperature. (c) Plasma frequency (ω_p) and Drude damping factor (Γ_D) of the HT-Ta film increase with the increase in temperature.

demonstrates significantly larger absorption in the near IR spectral range. In addition, the absorption spectra of the metasurface cover the whole solar spectrum [see Fig. 4(c)] that is suitable for solar energy conversion. The electric field distribution [see Fig. 4(b)] shows that when the wavelength of incident light is close to the ENZ wavelength of metal where ($\varepsilon_{metal} \rightarrow 0$), strong discontinuity of the electric field induces at the boundaries between air and metal ($E_{metal} = (\varepsilon_{air}/\varepsilon_{metal})E_{air}$). Consequently, a high-intensity electric field is localized near the top metallic layer that is 100 nm thick. Above the ENZ wavelength, metals are highly reflective ($\varepsilon_{metal} < 0$), and most of the field is confined outside the MIM structure. Enhanced absorption of the HT-RTMs highlights their effectiveness in several solar energy conversion applications.

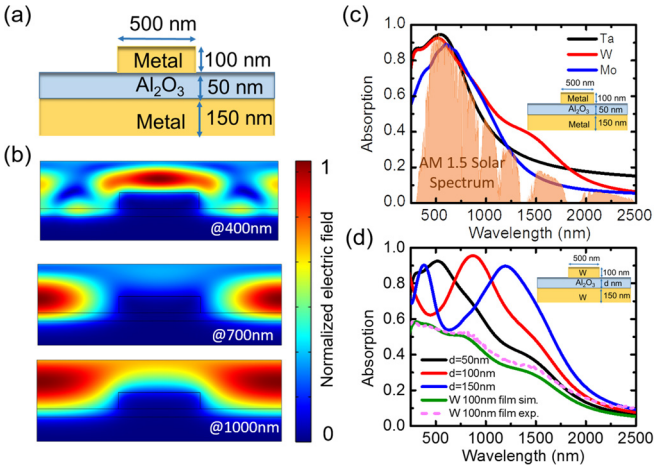

FIG. 4. (a) Schematic diagram of the unit cell of the metal–dielectric–metal based metasurface. (b) Electric field distribution throughout the Ta-based metasurface (air on the top of the metasurface) at different wavelengths of incident light, e.g., 400 nm, 700 nm, and 1000 nm. (c) Absorption of Ta, W, and Mo metasurfaces as a function of wavelength. Metasurface absorption is found to cover the full solar spectrum range at AM 1.5. (d) Absorption in the metasurface with varying dielectric medium (Al_2O_3) thicknesses [50 nm (black), 100 nm (red), and 150 nm (blue)] and compared with the 100 nm W thin film [simulated (green) and experimental (pink dotted line)].

The plasmonic properties of high-temperature (700 °C) deposited RTMs presented here mark a significant improvement in their optical properties compared to the previous reports on a polycrystalline sheet of RTMs and films deposited at 200 °C, which showed very little plasmonic response. On the other hand, RT-RTMs presented here show optical properties that are similar to the properties of the previous W and Mo films[45] deposited at 200 °C and annealed at 400 °C (see supplementary material 11). High-temperature depositions result in phase-pure highly crystalline RTMs with smooth surfaces that are as good as nitride-based alternative plasmonic materials. Indeed, the magnitude of ε_1 in the near-IR spectral range for HT-Ta is identical to that of TiN and ZrN, while its optical losses (ε_2) are slightly larger (see supplementary material 9). Similarly, the surface plasmon polariton (SPP) propagation length in HT-RTMs is about 10× larger than that in RT-RTMs (see supplementary material 8) and comparable to that in the nitrides. The figure of merit[58] (FOM) is another parameter that represents the quality of the plasmonic material. The FOM of HT-RTMs for the surface plasmon polariton (SPP) and localized surface plasmon polariton (LSPP) is found to be around 100 times and 10 times larger, respectively, compared to the values exhibited by RT-RTMs (see supplementary material 10). Also, the FOM of HT-RTMs is similar to that of the transition metal nitrides (TiN and ZrN) in the near-infrared (NIR) region. While reducing the optical losses[59,60] (ε_2) of the RTMs remains an important future avenue of research, the plasmonic properties of these metals and their ENZ characteristics presented here will no doubt attract researchers given their omnipresence in electronic and photonic industries for diverse applications.

In conclusion, high-temperature depositions inside the ultra-high vacuum are utilized to develop highly crystalline refractory transition metals (Ta, W, and Mo) as broadband ENZ and plasmonic materials for the visible-to-near-IR spectral applications. HT-RTMs are found to exhibit excellent plasmonic properties with ε_1 approaching that of other alternative plasmonic materials such as TiN and ZrN in the visible-to-near-IR range due to their high-crystalline quality and crystal structure. Temperature-dependent optical characterization reveals that the plasmonic and ENZ behavior is robust within the 100 K–700 K temperature range. The metasurface structure composed of RTMs is shown to exhibit larger absorptions in the entire solar spectral range. While the optical losses of RTMs are found to be larger than those of the noble metals and nitrides, development of refractory transition

metals (Ta, W, and Mo) marks a significant step in the research on alternative plasmonic and nanophotonic materials and will be useful for efficient absorbers, hot-electron generation, photo-catalysis, local heating, nanoparticle trapping, and other solar energy conversion devices.

See the supplementary material for details on growth details, ellipsometer measurements, and data fitting, temperature-dependent optical properties of W and Mo, x-ray diffraction, MIM cavity physics, surface plasmon polariton (SPP) propagation length, and comparison of the optical properties of RTMs with noble metal and transition metal nitrides.

K.C.M. and B.S. thank the International Center for Materials Science (ICMS) and Sheikh Saqr Laboratory (SSL) in JNCASR for support. B.S. thanks the Science and Engineering Research Board (SERB) of the Government of India, Start-Up Research Grant No. SRG/2019/000613, for partial financial support.

DATA AVAILABILITY

The data that support the findings of this study are available from the corresponding author upon reasonable request.

REFERENCES

[1]S. A. Maier, *Plasmonics: Fundamentals and Applications* (Springer, 2007).
[2]J. C. Ndukaife, V. M. Shalaev, and A. Boltasseva, Science **351**, 334 (2016).
[3]S. V. Boriskina, T. A. Cooper, L. Zeng, G. Ni, J. K. Tong, Y. Tsurimaki, Y. Huang, L. Meroueh, G. Mahan, and G. Chen, Adv. Opt. Photonics **9**, 775 (2017).
[4]N. Kinsey, C. DeVault, A. Boltasseva, and V. M. Shalaev, Nat. Rev. Mater. **4**, 742 (2019).
[5]G. Baffou and R. Quidant, Laser Photonics Rev. **7**, 171 (2013).
[6]M. L. Brongersma, N. J. Halas, and P. Nordlander, Nat. Nanotechnol. **10**, 25 (2015).
[7]J. C. Ndukaife, A. V. Kildishev, A. G. A. Nnanna, V. M. Shalaev, S. T. Wereley, and A. Boltasseva, Nat. Nanotechnol. **11**, 53 (2016).
[8]M. H. Javani and M. I. Stockman, Phys. Rev. Lett. **117**, 107404 (2016).
[9]S. Enoch, G. Tayeb, P. Sabouroux, N. Guérin, and P. Vincent, Phys. Rev. Lett. **89**, 213902 (2002).
[10]R. W. Ziolkowski, Phys. Rev. E **70**, 046608 (2004).
[11]A. Alù, M. G. Silveirinha, A. Salandrino, and N. Engheta, Phys. Rev. B **75**, 155410 (2007).
[12]J. Yoon, M. Zhou, M. A. Badsha, T. Y. Kim, Y. C. Jun, and C. K. Hwangbo, Sci. Rep. **5**, 12788 (2015).
[13]Y. Tian, F. P. García de Arquer, C. T. Dinh, G. Favraud, M. Bonifazi, J. Li, M. Liu, X. Zhang, X. Zheng, M. G. Kibria, S. Hoogland, D. Sinton, E. H. Sargent, and A. Fratalocchi, Adv. Mater. **29**, 1701165 (2017).
[14]M. L. Juan, M. Righini, and R. Quidant, Nat. Photonics **5**, 349 (2011).
[15]M. L. Juan, R. Gordon, Y. Pang, F. Eftekhari, and R. Quidant, Nat. Phys. **5**, 915 (2009).
[16]B. Hou, L. Shen, H. Shi, R. Kapadia, and S. B. Cronin, Phys. Chem. Chem. Phys. **19**, 2877 (2017).
[17]P. N. Dyachenko, S. Molesky, A. Y. Petrov, M. Störmer, T. Krekeler, S. Lang, M. Ritter, Z. Jacob, and M. Eich, Nat. Commun. **7**, 11809 (2016).
[18]C. C. Chang, W. J. M. Kort-Kamp, J. Nogan, T. S. Luk, A. K. Azad, A. J. Taylor, D. A. R. Dalvit, M. Sykora, and H. T. Chen, Nano Lett. **18**, 7665 (2018).
[19]M. Silveirinha and N. Engheta, Phys. Rev. Lett. **97**, 157403 (2006).
[20]D. C. Adams, S. Inampudi, T. Ribaudo, D. Slocum, S. Vangala, N. A. Kuhta, W. D. Goodhue, V. A. Podolskiy, and D. Wasserman, Phys. Rev. Lett. **107**, 133901 (2011).
[21]S. Campione, J. R. Wendt, G. A. Keeler, and T. S. Luk, ACS Photonics **3**, 293 (2016).
[22]O. Reshef, I. De Leon, M. Z. Alam, and R. W. Boyd, Nat. Rev. Mater. **4**, 535 (2019).
[23]N. Kinsey, C. DeVault, J. Kim, M. Ferrera, V. M. Shalaev, and A. Boltasseva, Optica **2**, 616 (2015).
[24]N. Engheta, Science **317**, 1698 (2007).
[25]P. B. Johnson and R. W. Christy, Phys. Rev. B **6**, 4370 (1972).
[26]W. Zhou, A. N. Rudenko, and S. Yuan, Adv. Electron. Mater. **6**, 1900860 (2020).
[27]M. Dadsetani and A. Ebrahimian, J. Electron. Mater. **45**, 5867 (2016).
[28]M. Z. Alam, I. D. Leon, and R. W. Boyd, Science **352**, 795 (2016).
[29]T. E. Tiwald, J. A. Woollam, S. Zollner, J. Christiansen, R. B. Gregory, T. Wetteroth, S. R. Wilson, and A. Powell, Phys. Rev. B **60**, 11464 (1999).
[30]R. Maas, J. Parsons, N. Engheta, and A. Polman, Nat. Photonics **7**, 907 (2013).
[31]W. Li, U. Guler, N. Kinsey, G. V. Naik, A. Boltasseva, J. Guan, V. M. Shalaev, and A. V. Kildishev, Adv. Mater. **26**, 7959 (2014).
[32]L. D. Yau and C. T. Sah, Appl. Phys. Lett. **21**, 157 (1972).
[33]V. J. Logeeswaran, N. P. Kobayashi, M. S. Islam, W. Wu, P. Chaturvedi, N. X. Fang, S. Y. Wang, and R. S. Williams, Nano Lett. **9**, 178 (2009).
[34]W. Chen, M. D. Thoreson, S. Ishii, A. V. Kildishev, and V. M. Shalaev, Opt. Express **18**, 5124 (2010).
[35]G. V. Naik, V. M. Shalaev, and A. Boltasseva, Adv. Mater. **25**, 3264 (2013).
[36]M. N. Gadalla, K. Chaudhary, C. M. Zgrabik, F. Capasso, and E. L. Hu, Opt. Express **28**, 14536 (2020).
[37]G. Subramania, A. J. Fischer, and T. S. Luk, Appl. Phys. Lett. **101**, 241107 (2012).
[38]B. Saha, G. V. Naik, S. Saber, C. Akatay, E. A. Stach, V. M. Shalaev, A. Boltasseva, and T. D. Sands, Phys. Rev. B **90**, 125420 (2014).
[39]S. Kalpakjian and S. R. Schmid, *Manufacturing Engineering and Technology*, 6th ed. (Prentice Hall, 2010).
[40]E. Kolawa, J. S. Chen, J. S. Reid, P. J. Pokela, and M. Nicolet, J. Appl. Phys. **70**, 1369 (1991).
[41]D. Hasan, P. Pitchappa, J. Wang, T. Wang, B. Yang, C. P. Ho, and C. Lee, ACS Photonics **4**(2), 302–315 (2017).
[42]J. H. Park, S. E. Han, P. Nagpal, and D. J. Norris, ACS Photonics **3**(3), 494–500 (2016).
[43]K. A. Arpin, M. D. Losego, and P. V. Braun, Chem. Mater. **23**, 4783 (2011).
[44]D. W. Juenker, L. J. LeBlanc, and C. R. Martin, J. Opt. Soc. Am. **58**, 164 (1968).
[45]M. P. Wells, R. Bower, R. Kilmurray, B. Zou, A. P. Mihai, G. Gobalakrichenane, N. M. Alford, R. F. M. Oulton, L. F. Cohen, S. A. Maier, A. V. Zayats, and P. K. Petrov, Opt. Express **26**, 15726 (2018).
[46]S. Gnanarajan, S. K. H. Lam, and A. Bendavid, J. Vac. Sci. Technol. A **28**, 175 (2010).
[47]P. Zheng, B. D. Ozsdolay, and D. Gall, J. Vac. Sci. Technol. A **33**, 061505 (2015).
[48]G. Mertler, M. Rey, and K. Reichelt, Nucl. Instrum. Methods Phys. Res. **192**, 535 (1982).
[49]G. Ehrlich and F. G. Hudda, J. Chem. Phys. **44**, 1039 (1966).
[50]R. L. Schwoebel and E. J. Shipsey, J. Appl. Phys. **37**, 3682 (1966).
[51]S. L. Lee, M. Doxbeck, J. Mueller, M. Cipollo, and P. Cote, Surf. Coat. Technol. **178**, 44 (2004).
[52]C. Y. Young, J. Phys. Chem. Solids **30**, 2765 (1969).
[53]W. E. Lawrence, Phys. Rev. B **13**, 5316 (1976).
[54]H. Reddy, U. Guler, A. V. Kildishev, A. Boltasseva, and V. M. Shalaev, Opt. Mater. Express **6**, 2776 (2016).
[55]S. T. Sundari, S. Chandra, and A. K. Tyagi, J. Appl. Phys. **114**, 033515 (2013).
[56]K. C. Maurya, V. M. Shalaev, A. Boltasseva, and B. Saha, Opt. Mater. Express **10**, 2679 (2020).
[57]B. J. Lee and Z. M. Zhang, J. Appl. Phys. **100**, 063529 (2006).
[58]M. G. Blaber, M. D. Arnold, and M. J. Ford, J. Phys. **22**, 143201 (2010).
[59]J. B. Khurgin and G. Sun, Appl. Phys. Lett. **96**, 181102 (2010).
[60]W. Walukiewicz, W. Shan, K. M. Yu, J. W. Ager, E. E. Haller, I. Miotkowski, M. J. Seong, H. Alawadhi, and A. K. Ramdas, Phys. Rev. Lett. **85**, 1552 (2000).